Contribution to the glaciology of northern Greenland from satellite radar interferometry

E. Rignot[1], S. Gogineni[2], I. Joughin[1], W. B. Krabill[3]

[1] *Jet Propulsion Laboratory, California Institute of Technology, Pasadena 91109, California, U.S.A.*

[2] *Radar Systems and Remote Sensing Laboratory, The University of Kansas, Lawrence 66045, U.S.A.*

[3] *NASA GSFC Wallops Facility, Laboratory for Hydrospheric Processes, Wallops Island 23337 Virginia, U.S.A.*

Abstract. Interferometric synthetic-aperture radar (InSAR) data from the ERS-1 and ERS-2 satellites are used to measure the surface velocity, topography, and grounding-line position of the major outlet glaciers in the northern sector of the Greenland Ice Sheet. The mass output of the glaciers at and above the grounding line is determined and compared with the mass input. We find that the grounding-line output is approximately in balance with the input, except for the three largest glaciers for which the mass loss is 4±3 km^3 ice a^{-1} or 11±8 percent of the mass input. Along the coast, we detect a systematic retreat of the grounding lines between 1992 and 1996 with InSAR, which implies that the outlet glaciers are thinning. The inferred coastal thinning is too large to be explained by a few warm summers. Glacier thinning must be of dynamic origin, i.e. caused by spatial and temporal changes in ice velocity.

Iceberg production from the glaciers is uncharacteristically low. It accounts for only 8 percent of the ice discharge to the ocean. About 55 percent of the ice is lost through basal melting (5-8 m ice a^{-1} on average) from the underside of the floating glacier tongues that are in contact with warm ocean waters. Mass losses are highest in the first 10 km of floating ice, where ice reaches the

greatest depths and basal melting is three times larger than on average. Only a small increase in basal melting would suffice to desintegrate the floating glacier tongues.

1 Introduction

Early in this century, the first observations of northern Greenland glaciers were made using watches, sextant, sketch maps and photography [*Koch*, 1928]. These observations revealed the presence of large sectors of floating ice, consolidated by the presence of nearly permanent fjord ice. Aerial photography and field studies from the 1950s showed that the glacier fronts were slowly retreating and thinning, especially in the case of tide-water glaciers [*Davies and Krinsley*, 1962]. Little information was available, however, on the rates of glacier thinning.

More recently, *Higgins* [1988, 1991] reported estimates of ice-front velocity and calf-ice production for northern Greenland. *Reeh* [1985] found that ice produced by calving was low compared with that estimated for an ice sheet in mass balance. This suggests that large uncertainties remain in the determination of the mass budget of the northern sector of the ice sheet, which represents 25 percent of the ice-covered area in Greenland.

Here, we present a study of northern Greenland glaciers conducted using spaceborne interferometric synthetic-aperture radar (InSAR) data collected between 1992 and 1996 by the European Space Agency's (ESA) Earth Remote Sensing Satellites ERS-1 and ERS-2. The InSAR data were used to map the detailed topography and vector flow of the ice sheet [*Joughin et al.*, 1998; *Mohr et al.*, 1998], and detect the tidally-induced vertical motion of floating ice [*Rignot*, 1996] over large sectors (several hundred km). The InSAR results were combined with Airborne Topographic Mapping (ATM) surface elevation data [*Krabill et al.*, 1999], ice-sounding radar data (ISR) [*Chuah et al.*, 1996], a new digital elevation model (DEM) of Greenland [*Ekholm*, 1996; Bamber et al., 2001], and a new map of snow accumulation [*Bales et al.*, 2000]. This allowed to obtain a more precise estimate of the mass balance of the northern sector of the Greenland Ice Sheet and to detect coastal thinning/thickening trends of the glaciers via the monitoring of their grounding-line positions [*Rignot, 1998a*]. The paper summarizes our study, and includes new ISR and ATM data collected in 1999, the analysis of additional glaciers, the detection of grounding-line migration on all floating ice tongues, and vector maps of ice velocity, that were not included in [*Rignot*, 1996; *Rignot et al.*, 1997a and b; *Rignot et al.*, 2000]. We conclude on the probable state of mass balance of the northern sector of the Greenland Ice Sheet, and on the implications of the InSAR results.

2 Study area

Figure 1 shows a composite SAR image mosaic of the outlet glaciers considered in this study. Because our primary goal is to determine the mass balance of the northern sector of the ice sheet as a whole, we only studied the ice discharge from the largest outlet glaciers. Glaciers draining from local ice caps in Ingelfield, Nyboe, Peary and Kronprins Christian Land, and alpine glaciers draining from Nansen and Peary Land [*Weidick*, 1995] were not included. The study area is about 500,000 km^2 in size. It extends from Harald Moltke Glacier (76.5 N, 68 W) near Thule Air Base, to Storstrømmen Gletscher (76.5 N, 23 W) in the east. Most outlet glaciers in that sector develop a floating glacier tongue. Few floating glacier tongues exist on the east coast south of Storstrømmen.

3 Methods

3.1 Interferometry products

The theory of producing SAR interferograms of glaciated terrain has been described elsewhere [*Rignot et al.*, 1995; *Joughin et al.*, 1995; *Rignot* , 1996; *Joughin et al.*, 1996, 1998 and 1999; *Mohr et al.*, 1998] and will not be repeated here. We will only summarize the salient features of our methodology.

The first InSAR observations of northern Greenland were collected in the winter of 1992 by ERS-1, then on a three-day exact-repeat orbit cycle. A larger volume of data was acquired in the winter of 1995-1996 by ERS-1 and ERS-2 flying in tandem mode: i.e., ERS-2 following ERS-1 along the same orbit with a one-day time difference. Almost no tandem data were acquired after 1996.

Double-difference SAR interferograms were used to generate topographic maps of the ice sheet with a vertical precision no better than $\pm$ 20 m. These maps helped correct single-difference SAR interferograms for the effect of topography to estimate ice velocity. On floating glacier ice, satellite radar altimetry provides better topographic maps, because InSAR is contaminated by oceanic tides. For this reason, we used the Greenland DEM to correct single-difference SAR interferograms for topography on floating ice and also to infer ice-shelf thickness from ice-shelf surface elevation. Bamber et al. [2001] derived their DEM by combining radar altimetry with GPS surveys, airborne laser measurements, and aerial photography.

We combined single-difference SAR interferograms collected along ascending and descending tracks to produce vector maps of ice motion, except where no ascending tracks were collected (from Harald Moltke to Humboldt Gletscher). We assumed that ice flows parallel to the ice sheet surface, which is a reasonable approximation for polar glaciers. On floating ice, tidal motion was removed using the method described in *Rignot et al.*, [2000], which employs tidal predictions from the FES95.2 tidal model [*Le Provost et al.*, 1998] combined with a quadruple-difference SAR interferogram. Comparisons of InSAR-derived motion vectors with GPS data in various areas of grounded ice [*Rignot et al.*, 1995; *Mohr et al.*, 1998; *Joughin et al.*, 1999] suggest that, in most favorable conditions, ice velocity is measured with a precision of 2-5 m a^{-1}. An example vector map of ice velocity is shown in Fig. 2.

Rignot [1998a] showed that grounding-line positions can be mapped with InSAR with a horizontal precision of 20-50 m, which is one to two orders of magnitude better than that in prior studies [*Rignot* , 1998b]. Grounding-line positions, however, migrate back and forth with ocean tide, over a rough bed. This limits the precision of mean-sea-level grounding-line mapping to 100-200 m (assuming ± 1 m oceanic tide and one percent thickness slope), unless multiple interferograms are analyzed. Using this approach, we detected grounding-line migration between 1992 and 1996 and converted the results into thinning/thickening rates using surface slope measured by ATM and thickness slope measured by ISR.

3.2 Ice thickness

We used both measured and estimated ice thickness to compute the ice flux. The measured thicknesses were used primarily to compute mass flux using a transverse ISR profile upstream of the grounding line. These data were collected with a 150-MHz coherent radar, operated on an aircraft equipped with GPS receivers. The uncertainty in ice thickness is 10 m [*Rignot et al.*, 1997b]. Only a few ice thickness measurements were made across the glacier at grounding lines because of the inherent difficulties of flying the aircraft across deep fjords, and processing radar echoes in the proximity of steep rock and ice faces. We estimated the grounding-line thickness from ice-shelf elevation from DEM or ATM data, assuming hydrostatic equilibrium of the ice. We used a multiplicative factor of 9.115 to convert grounding-line elevation to ice thickness.

In Table 1, we compare the results with ISR at the point of crossing with the grounding line. The average error is 8 ± 13 percent of the actual thickness. Large deviations (≈ 30 percent) exist on a few glaciers (Hagen Brae and Storstrømmen), which are not in equilibrium because they are surge-type glaciers. An ad-hoc correction (i.e., an absolute bias and a new multiplicative factor) is applied on the DEM to reduce the uncertainty in derived thickness. The precision of the corrected thickness is estimated to be about 20 to 50 m (last column of Table 1, and Fig. 3).

3.3 Ice fluxes

We calculated the ice flux both at the grounding line and upstream of the grounding line when transverse ISR data were available. We computed the flux at two locations to increase confidence in the estimates of grounding-line discharge and to estimate the glacier mass balance at higher elevation, where ice dynamics and ablation effects are presumably less significant.

We calculated ice-front fluxes for a few glaciers, and also compiled published data on few others. The difference in ice flux between the grounding line and the ice front, divided by the ice-shelf area in between, yields an estimate of the net balance of floating ice (Table 5). Comparing the result with accumulation minus surface ablation on the floating ice tongue, we deduced an average basal melting rate under steady state conditions. Similarly, we calculated the average basal melting rate for the first 10 km of floating ice (Table 5), where basal melting is higher. If the floating ice tongues are not in steady state and are for instance thinning 1-2 m a^{-1}, conservation of mass dictates that basal melting should actually exceed the steady-state rates listed in Table 5 by the same amount.

For a typical grounding-line thickness of 600 m with an uncertainty of 30 m, and a grounding-line velocity of 1000 m a^{-1} with an uncertainty of 4 m a^{-1}, the error in mass flux is 5 percent and the error in steady-state basal melting is 12 percent (10 percent uncertainty for surface melt on ice shelves).

3.4 Glacier topography

The ATM laser instrument on the aircraft flying at 500 m above the ice surface scans over a 50-m swath, centered at about the nadir point on the ice surface. ATM surface elevations are reported to have a height measurement uncertainty of about 10 cm [*Krabill et al.* 1999]. We used these data to identify hydrostatic equilibrium of the ice (Table 1 and Fig. 3 and 4) in the proximity of the

InSAR-derived grounding lines. A few outlet glaciers were also surveyed repeatedly to measure elevation changes between 1994 and 1999.

We utilized the Greenland DEM to delineate drainage basins from the end points of the flux gates, following the line of steepest slope. We matched the end points of the grounding line and ISR flux gates along flow lines to conserve mass between flux gates. Radar altimeters do not measure surface slope well near the ice sheet margin, i.e. right above the grounding line. Because of this, we used clearly-defined flow-line features visible in the SAR imagery to initiate the drainage boundaries at low elevation. This procedure was extended to high elevation until the line of steepest slope derived from the DEM was found to be well aligned with flow-line features in the SAR imagery.

3.5 Mass accumulation

Annual precipitation is low in northern Greenland, $\approx$ 100-300 mm water equivalent in the humid coastal areas, and less than 100 mm in the interior [*Weidick*, 1995]). The 1993-1994 German expedition in east Greenland [*Friedman et al.*, 1995] revealed that *Ohmura and Reeh* [1991] overestimated accumulation in the north. This was confirmed with recent ice cores [*Bales et al.*, 2000]. In the case of the combined drainage basin from the six largest northern glaciers, the new accumulation numbers are 11 percent lower than those employed in [*Rignot et al.*, 1997a], which were based on *Ohmura and Reeh* [1991]. In *Rignot et al.* [2000], we employed a preliminary version of the new accumulation map that is about 4 percent larger than that in this study. We estimate that an accumulation uncertainty of 5 percent is a reasonable assumption for the entire domain of study, but the uncertainty may be larger than 10 percent over small areas.

3.6 Mass ablation

Few studies of mass ablation have been conducted in the north ([*Nobles*, 1960; *Goldthwait*, 1971] at "Red Rock" near Thule Air Base; [*Høy*, 1970] in Christian Erichsen Iskappe in Peary Land (lat 77^o N, long 25^o W); [*Lister*, 1958] on Britannia Glacier, in Dronne Louise Land (lat 77^o N, long 24-25^o W); [*Konzelmann and Braithwaite*, 1995] in Kronprins Christian Land (KPCL) (lat 80 N, long 24 W); [*Braithwaite et al.*, 1998] in Hans Tausen Iskappe (HTI) (lat 83 N, long 36 W), and [*Bøggild et al.*, 1994] on Storstrømmen (lat 77 N, long 23 W)]). The results suggest large inter-glacier variability in radiation budget: the degree-day factor for ice at KPCL is 9.8$\pm$0.9 versus 5.9$\pm$0.6 at HTI.

In a prior assessment of ice sheet mass balance, we used *Reeh*'s [1991] degree-day model with a degree-day factor of 9.8-mm/deg/day for ice [*Braithwaite*, 1992] and 3.0 mm/deg/day for snow. These values are higher than those derived for western Greenland [*Braithwaite*, 1995, 1996] because cloud cover is reduced in northern Greenland [*van der Wall*, 1996].

In Table 2, we adjusted the degree-day factor for each glacier to reproduce either a published value of the glacier equilibrium line altitude (ELA), or its presumed location based on ERS imagery. This is based on a method discussed in *Joughin et al.* [1999] and *Rignot et al.,* [2000]. The ELA depends on the degree-day factor for snow, which we assume to be equal to 40 percent the degree-day factor for ice, following *Braithwaite* [1996]. Changing the degree-day factor for snow from 0.3 (high value) to 0.18 (low value) decreases the ELA by about 200 m. The ELAs in Table 2 are not known with a precision better than 100 m vertical (10 km horizontal). This level of precision, however, is sufficient to reduce the uncertainty in surface melt to an acceptable level.

Most glaciers fit the higher degree-day factor, except three. In the case of Nioghalvfjerdsbrae, we calculate a net ablation of 2.8 km^3 ice a^{-1} for the floating tongue using the lower degree-day factor, compared to 3.0 km^3 ice a^{-1} estimated by *Reeh et al.* [1999] using unpublished in-situ measurements. Our new estimates of surface ablation should therefore have an uncertainty of about 10 percent for the entire study area. Larger errors (20 to 30 percent) are not be excluded on small areas. While this uncertainty is large, it has a limited impact on the mass balance estimates. In Table 3, ablation accounts for 10 percent of the mass budget, hence yields only a 1-percent uncertainty in mass balance. In Table 4, ablation is 28 percent of the mass budget and contributes a 3-percent uncertainty. By measuring ice fluxes at and upstream of the grounding line, we avoid dealing with the bulk of surface ablation that prevails at lower elevation.

Overall, the balance flux for each glacier is not known with a precision better than 10 percent, but the balance flux for the entire sector of study should be reliable at the 6-percent level (5 percent for accumulation, 3 percent for ablation). The mass balance estimates should therefore be accurate at the 8-percent level.

4 Results of the glacier survey

Here, we describe the mass balance, grounding-line migration and basal melting results obtained from each glacier, starting from the west and moving toward the east. For some glaciers, no results are included in Tables 3-6, for reasons described below, but we discuss new information relevant to their state of mass balance.

4.1 Harald Moltke, Heilprin and Tracy glaciers.

The 1996 ERS data show no floating section for these three glaciers. This is consistent with the observations of *Koch* [1928] in the case of Harald Moltke, but it is contrary to *Davis and Krinsley* [1962] reports on Heilprin and Tracy glaciers. These two glaciers have probably thinned and retreated considerably since the 1950s.

Harald Moltke is a surge-type glacier [*Mock*, 1966]. It drains from local ice domes, not from the inland ice as presumed in the past. Hence, it is not included in Tables 3-6. At the ice front, it is 5-km wide, 400-m thick and flows at 90 m a^{-1}. This yields a mass flux which is 25 percent lower than the balance flux at that location. At the ISR flux gate located 30 km upstream, ice discharge is 26 percent larger than the balance flux. This balance pattern suggests that ice accumulates between the front and the ISR gate, perhaps in prelude to the next surge.

Kollmeyer [1980] documented a large retreat for Heilprin and Tracy glaciers, with Tracy Gletscher retreating the most (7 km between 1892 and 1959). The ice discharge in Table 3 is lower than that estimated by *Weidick*, [1995], perhaps because the glaciers slowed down in recent times. It is significantly larger (33 percent) than the balance discharge, however, which suggests significant thinning in this sector of the ice sheet.

4.2 Humboldt Gletscher.

This glacier is 110-km wide at the calving front, with a low rate of movement. ERS data confirm earlier observations [*Kollmeyer*, 1980] that most of the glacier front is grounded, except for a few places that float at high tide in the southern sector. The northern sector flows faster and develops a permanent floating section (Fig. 4a). The glacier is close to a state of mass balance at the ISR flux gate (Table 3). A division of the glacier drainage into a northern and southern sectors, however, reveals that the northern sector exhibits a more negative mass balance than the southern sector (not shown in Table 3). This result is consistent with ATM measurements which show more pronounced thinning in the north than in the south [*Abdalati et al*, 2001].

The grounding line retreated 1 km between 1992 and 1996, which implies a thinning of 1.7 m ice

a^{-1} (Table 6). The ATM measurements collected 20 km further north revealed a 1±0.5 m ice a^{-1} thinning rate, which is consistent with our estimate. Humboldt Gletscher is therefore thinning in the north, where ice flows fast, and closer to equilibrium in the south, where ice moves slowly.

4.3 Petermann Gletscher

Petermann Gletscher is a fast-moving glacier that develops a 20-km wide by 70-km long floating tongue. We improved our earlier estimates of its grounding-line flux by using a vector map of ice velocity (Fig. 2) and a corrected DEM (Table 1). The new estimate is in agreement with that computed using a transverse ISR profile collected in May 1999, a few km upstream of the grounding line (Fig. 4b). The glacier mass balance is -7 percent of the balance flux at the grounding line (Table 4), and -5 percent at the ISR flux gate (Table 3).

The grounding line retreated 450±100 m between 1992 and 1996 at the crossing point with the 1995 ISR data, which implies a thinning rate of 1.3 m ice a^{-1} (Table 6). The average retreat rate across the glacier width is 270 m, which implies 0.8 m ice a^{-1} thinning.

The line of first hydrostatic equilibrium of the ice is found 1.5 km downstream of the InSAR-derived grounding line. Similar offsets are found for other glaciers. In 1999, the limit of hydrostatic equilibrium migrated south of its 1996 position (Fig. 4b), which suggests that the grounding line continued its slow retreat.

The calf-ice production from this glacier is 20 times lower than its grounding line discharge (Table 4). The net balance of the floating ice tongue is -8.4 m ice a^{-1} (Table 5), of which -2.2 m ice a^{-1} is due to surface runoff plus accumulation, and the rest is due to basal melting [*Rignot*, 1996]. Overall, 70 percent of the ice is lost from bottom melting, 25 percent from surface melting, and the rest from calving (icebergs). This division of process differs markedly from that of glaciers located further south, where ice discharge is evenly partitioned between surface melting and calving [*Reeh et al.*, 1999].

4.4 Newbugt glacier, Steensby Gletscher

The 2-km-wide Newbugt glacier flows between Hall and Nyeboe Land [*Higgins*, 1991], with minimal ice discharge. We found no floating section in 1996 whereas *Higgins* [1991] reported that the frontal 1 km was afloat. The ice velocity decreased from 35-45 m a^{-1} in the 1970s [*Higgins*, 1991] to 19-20 m a^{-1} in 1996. The glacier is likely in a state of retreat.

The 4.5-km-wide Steensby Gletscher has a mass budget close to zero (Table 4). Its 1996 velocity is similar to that measured by *Higgins* [1991] in the 1970s. Its grounding line advanced slightly (Fig. 4c), which implies a slight thickening of the glacier (Table 6). The average basal melting rate of its floating tongue is similar to that estimated on other glaciers (Table 5).

4.5 Ryder Gletscher

This 8-km-wide glacier drains into Sherard Osborn Fjord. *Davies and Krinsley*, [1962] reported a large retreat of the glacier prior to 1947, with further retreat by calving between 1947 and 1958. The glacier experienced a mini-surge in 1995, which more than tripled its ice velocity on October 26/27 1995 [*Joughin and others,* 1996]. By November 8/9, the velocity returned to normal values observed on September 21/22. Additional data subsequently revealed that the glacier velocity was still normal on Oct. 10/11, 1995. The mini-surge of 1995, therefore, lasted about 3.7 weeks.

Two successive, large, transverse ridges revealed by the ISR data (one ridge is shown in Fig. 3c at -3 km, another in *Joughin et al.,* [1999]) obstruct the glacier flow into the fjord. This unusual bed configuration probably plays a major role in the ponding of basal melt water upstream of the grounding line, which was suggested to be responsible for the pulsing (surge) behavior of the glacier.

If the glacier were to triple its velocity for four weeks every year, it would discharge 15 percent more ice than listed in Table 4. This would reduce its positive mass balance from 43 to 28 percent. The glacier would need to surge for longer time periods (12 weeks) every year to be in balance with the mass input listed in Table 4. At the ISR flux gate, the glacier balance reduces to 17 percent (Table 3).

The grounding line retreated 4.2 km between 1992 and 1996, which is the largest retreat in our study area (Fig. 4d). The retreat implies a thinning of 4 m ice a^{-1} (Table 6). Most likely, the glacier lost a large quantity of ice during the surge. At the location of the 1996 grounding line, the ATM data indicates a 2-m thinning between 1997 and 1999. In 1999, the line of hydrostatic equilibrium migrated upstream of its 1997 position (Fig. 4d), which also suggests glacier thinning. One possible way to reconcile the thickening indicated by the ice fluxes with the thinning indicated by InSAR and ATM is that the glacier drainage basin is overestimated in the DEM (see next sub-section).

4.6 C.H. Ostenfeld Gletscher, Harder and Brikkerne glaciers.

These glaciers drain into Victoria Fjord (Fig. 4e). Ostenfeld Gletscher is the largest and most active glacier. Its 7-km-wide disconnected floating segment moved at 800 m a^{-1} in 1996, as in the early 1960s, with a similar ice tongue configuration [*Higgins and Weidick*, 1988]. Brikkerne Gletscher, which flows from the north east, is a surge-type glacier. The 1996 velocity of its three branches is lower than that recorded in 1978, but comparable to that recorded in 1963, prior to a surge. Harder and Brikkerne Gletscher nourish from a local ice dome, not from the inland ice, and are not included in Tables 3-6.

The mass balance of Ostenfeld Gletscher is largely negative: -71 percent at the grounding line (Table 4) and -50 percent at the ISR flux gate (Table 3). Its drainage basin is bound by a dome to the north, and Ryder Gletscher to the south. If the divide between Ryder and Ostenfeld glaciers is correct, Ostenfeld Gletscher must experience massive thinning at present. Most likely, some of the flow attributed to Ostenfeld Gletscher belongs to Ryder Gletscher. The combined mass budget of the two glaciers is close to balance in Table 4.

The grounding line of Ostenfeld Gletscher retreated 500$\pm$300 m between 1992 and 1996 (Fig. 4e), which implies 5 m ice a^{-1} thinning. This result confirms the probable state of retreat of this glacier, independent of its mass input.

4.7 Jungersen, Henson, Marie Sophie, Academy and Hagen glaciers

The importance of Jungersen and Henson glaciers was exaggerated in earlier work [*Koch*,, 1928]. Both glaciers exhibit floating sections, with minimal discharge. The drainage basins are not defined clearly in this sector of the ice sheet.

Marie Sophie and Academy glaciers discharge into Independence Fjord and exhibited no floating section in 1996. Marie Sophie Gletscher reduced its velocity by half since the 1970s [*Higgins*, 1991], while the 8.5-km-wide Academy Gletscher maintained a velocity of 270 m a^{-1}. The mass budget of Academy Gletscher is largely positive, which is not consistent with the state of retreat reported by *Davies and Krinsley* [1962]. The divide between Academy Gletscher and Hagen Brae, however, is uncertain since the two glaciers merge at the location of the ISR profile, at about 1000 m elevation (Fig. 1).

Hagen Brae is a 10-km-wide outlet glacier whose ice front is dammed by two islands. The glacier overrides a transverse ridge at the grounding line. The 1996 ice front velocity of 94 m a^{-1} is considerably lower than the 510-540 m a^{-1} reported by *Higgins*, 1991], which suggests anomalously low glacier velocity in 1996. The 1996 glacier velocity decreases from the ELA to near-zero values at the ice front, similar to the velocity profile of Storstrømmen, a surge-type glacier in the north east [*Reeh et al.*, 1994]. As a result, the glacier mass budget is largely positive at the grounding line, and closer to zero at the ISR flux gate (Tables 3-4). These observations suggest that Hagen Brae is a surge-type glacier, which surged in the 1970s, and is now in a quiescent mode.

The grounding line of Hagen Brae retreated 400 m between 1992 and 1996 (Fig. 4f), which translates into a 1.6 m ice a^{-1} thinning, comparable to that measured with ATM (Table 6). Because the glacier is nearly stagnant at the grounding line, it is probably thinning at its ablation rate.

4.8 Nioghalvfjerdsbrae and Zachariae Isstrøm.

This sector of northern Greenland was discussed by [*Thomsen et al.*, 1997; *Rignot et al.*, 1997a, *Joughin et al.*, 2001; *Reeh et al.*, 1999]. A major retreat of the outlet glaciers must have taken place in the first half of the century since Zachariae Isstrøm and Nioghalvfjerdsbrae used to form coalescent ice tongues into an ice shelf filling up Nioghalvfjerdsfjorden [*Weidick*, 1995]. These glaciers also serve as outlets for the north-east ice stream, an unusual flow feature in Greenland.

The mass budget of Nioghalvfjerdsbrae is negative (Tables 3-4), whereas the mass budget of Zachariae Isstrøm is close to zero. The divide between Nioghalvfjerdsbrae and Zachariae Isstrøm is difficult to define with certainty for hundreds of km upstream of the grounding lines. A more reliable indication of the mass balance of these glaciers is that their combined ice discharge exceeds the balance flux by 12 percent. They are therefore likely losing mass at present.

The grounding line of Nioghalvfjerdsbrae retreated 400-600 m at the glacier center between 1992 and 1996 (Fig. 4g), which implies 1.6 m ice a^{-1} thinning (Table 6). On the southern flank of

Nioghalvfjerdsbrae, hydrostatic equilibrium migrated inland in 1999 compared to 1996 (Fig. 4g), i.e. the grounding line probably continued to retreat after 1996. Similarly, on Zachariae Isstrøm, for which no InSAR data exist prior to 1996, the region of hydrostatic equilibrium migrated inland between 1995 and 1999 (Figs. 3d and 4h), which suggests glacier thinning.

4.9 Storstrømmen and L. Bistrup Brae

The velocity of Storstrømmen was deemed to be considerable by *Higgins* [1991] (1.8 km a^{-1}), but the glacier was found to be stagnant in the 1990s [*Mohr et al.*, 1998]. Storstrømmen is a surge-type glacier. Its current low level of ice discharge explains its largely positive mass budget (Tables 3-4).

The grounding line of Storstrømmen exhibits a mixture of retreat and advance (Fig. 4i). The retreating sector has a very low surface slope, which implies no thinning (Table 6). The advancing southern sector thickened slightly between 1992 and 1996. The ATM instrument measures thinning of 2 m ice a^{-1} between 1994 and 1999. Because the velocity is low, the glacier is likely thinning at its ablation rate. Surface ablation varies strongly from year to year [*Bøggild et al.*, 1994], and was unusually high in 1997, which was a record warm year in northern Greenland (K. Steffen, pers. comm. 1999). The difference in retreat rate between ATM and InSAR may therefore merely reflect inter-annual changes in surface melt. On the slow-moving L. Bistrup Brae, both ATM and InSAR indicate thickening at the grounding line.

5 Discussion

Mass balance. The eleven glaciers listed in Table 3 total a discharge of 62 km^3 ice a^{-1} compared to a balance flux of 60 km^3 ice a^{-1}, which means that the northern sector of the Greenland Ice Sheet is approximately in balance. The mass budget is similarly close to zero at the grounding line

(Table 4). Numerous glaciers, however, exhibit positive or negative mass balance anomalies. Positive anomalies are often associated with documented or suspected surging behavior. Some negative anomalies result from uncertainties in drainage boundaries between neighboring glaciers. If we included more realistic estimates of ice discharge from surge-type glaciers, positive anomalies would be reduced, but the total mass budget would not change significantly.

The three largest glaciers, Petermann Gletscher, Nioghalvfjerdsbrae and Zachariae Isstrøm control 90 percent of the ice discharge in this sector. Their mass budget is -10$\pm$8 percent of the balance discharge at the ISR flux gate and -11$\pm$8 percent at the grounding line. The mass budget of the larger glaciers is therefore negative.

If we ignore the mass budget of the smaller and surge-type glaciers, the northern sector of the ice sheet appears to be loosing mass at a rate of about 4$\pm$3 km^3 ice a^{-1}. This rate of mass loss contributes 1/100 th of millimeter global sea level rise [*Jacobs et al.*, 1996], which is negligible. Similarly, it contributes negligible ice sheet thinning if spread uniformly over the entire drainage area. Yet, it could produce meter-scale glacier thinning if concentrated near the coast, e.g. over a 50-km wide region upstream of the grounding line. The results of Krabill et al. [1999] indeed suggest negligible mass imbalance of the ice sheet interior, but thinning near the coast.

Coastal thinning. The detection of grounding-line migration with InSAR reveals that all glaciers developing a floating ice tongue retreated between 1992 and 1996, except slow-moving L. Bistrup Brae and advancing Steensby Gletscher. The retreat rate varies from several hundred m a^{-1} up to 1 km a^{-1}, and converts into thinning of 1 to 2 m ice a^{-1}.

The magnitude of ice thinning inferred from the grounding line retreat is large compared to surface ablation (typically less than 1 m ice a^{-1} at the grounding line [*Thomsen et al.*, 1997]). The glacier retreat is therefore unlikely to be explained by enhanced surface melt between 1992 and 1996, from either warmer air temperatures or a longer melt season. Glacier thinning must therefore also be of dynamic origin.

Glacier ice may thin from enhanced longitudinal stretching, e.g. if the glacier velocity increases over time and space. In the case of the three largest glaciers discussed above, an ice thinning of 1.5 m ice a^{-1} would result from a longitudinal stretching of the ice by 0.0025 a^{-1} if the grounding-line ice thickness is 600 m. Over a distance of one glacier width (20 km), this represents a 50 m a^{-1} increase in ice velocity, which is only 4 percent of the ice velocity at the grounding line. Measuring such an acceleration, or possibly lower if enhanced surface melt also contributes to glacier thinning, should be investigated in the future. An increase in coastal velocity of the outlet glaciers compared to the inland ice would cause coastal thinning and grounding-line retreat, while maintaining the ice sheet interior close to a state of mass balance.

If the thinning rates inferred from InSAR had prevailed over one century, the ice tongues of northern Greenland would not have survived and we should have witnessed a major retreat of the glacier fronts. Petermann Gletscher, for one, did not experience a major retreat, although earlier reports suggested a much rougher surface for its ice tongue than at present [*Koch*, 1928]. Retreat of floating glacier tongues and sea ice has been more obvious in the north east [*Weidick, 1995*]. One possibility, given the historical evidence for glacier-front retreat, is that ice thinning and glacial retreat must have accelerated in the last few decades.

Basal melting. The study reveals the magnitude and extent of basal melting on northern Greenland floating ice tongues. Basal melt rates underneath the Ross and Filchner-Ronne ice shelves average a few tens of cm ice a^{-1} [*Jacobs et al.*, 1996]. In northern Greenland, the average melt rates are ten times larger. Not only is basal melting high, but it is also the dominant form of mass ablation. Basal melting averages 5-8 m ice a^{-1} on the floating tongues. In the proximity of the grounding line, the rates are three times larger (Table 5). A higher melt rate is expected in these regions, because the ice draft reaches greater depths, and melting is facilitated at greater depths due to the pressure dependence of the ice melting point [*Jenkins and Doake*, 1991].

Near the grounding line, basal melting will influence ice flow in three ways. If basal melting is too large to maintain the ice in a state of mass balance, steeper surface gradients will be generated at the grounding line, which will increase the driving stress. Higher deviatoric stress gradients across the grounding line will also contribute to softening of the ice [*Huybrecht*,, 1990]. Finally, the buttressing floating tongues will offer less resistance to inland outflow as they thin, which may increase ice discharge. High basal melting could therefore rapidly melt the floating tongues and perhaps cause more rapid discharge of inland ice.

The influence of basal melting on ice sheet evolution has only been investigated for the Antarctic ice sheet, generally for modest levels of basal melting [*Huybrecht and de Wolde*, 1999]. The values of basal melting recorded here, in the proximity of grounding lines, are two to five times larger than that in simulations. Also, those simulations indicated that changing the ocean conditions underneath the floating tongues is a far more efficient way to collapse ice shelves than increasing surface melt due to warmer air temperatures. Here, a 10 percent increase in bottom melting near the grounding line would have drastic consequences on the sustainability of floating ice tongues: the floating sector of Petermann Gletscher would disappear in 30 years. In contrast, a 10 percent increase in surface melt, from warmer or longer summers, is unlikely to disintegrate the floating tongues.

6 Conclusions

The advents of InSAR and other new technologies have permitted a major improvement in our knowledge of ice dynamics and mass balance of northern Greenland glaciers. From these data, we have established a modern estimate of the mass budget of these glaciers, which is close to balance, except in the case of the larger glaciers for which the mass budget is negative. The detection of a systematic grounding-line retreat of the outlet glaciers provides strong evidence of their slow retreat and thinning along the coast, independent of their mass input and output. The thinning rates inferred from the 1992-1996 grounding-line retreat are large. They cannot be explained by a few warmer or longer summers, which suggests that ice thinning is also of dynamic origin. Coincidentally, evidence for coastal dynamic thinning is more pronounced in other parts of Greenland [*Thomas et al.*, 2000].

Numerous surge-type glaciers are present in northern Greenland, despite its dry, cold climate. These glaciers contribute less than 10 percent of the total ice discharge. The resulting positive mass budget anomalies, however, emphasize the importance of gathering information on ice dynamics in order to interpret the results from satellite radar and laser altimeters. Similarly, the interpretation of negative anomalies requires information on temporal and spatial changes in ice velocity.

InSAR has also allowed a systematic assessment of basal melting on the northern floating tongues. The result is that the inferred melt rates exceed those recorded on large Antarctic ice shelves by one order of magnitude. It is neither clear how such high basal melting rates can be sustained over time by the surrounding ocean waters, nor how the floating tongues can or cannot survive in such an environment. In-situ, timely observations of ocean conditions beneath the floating tongues are needed to confirm and better understand the remote sensing results.

Acknowledgements This work was performed at the Jet Propulsion Laboratory, California Institute of Technology, under a contract with the National Aeronautics and Space Administration, Polar Research Program. We thank R.H. Thomas and an anonymous reviewer for their thoughtful reviews of the manuscript, C. Werner for use of his SAR processor, and the members of the PARCA project for numerous and fruitful intellectual interactions over the years.

References

Abdalati, W. and 9 others, Outlet glacier and margin elevation changes: near-coastal thinning of the Greenland ice sheet, *J. Geophys. Res.*, in press.

Bales, R.C., J. R. McConnell, E. Mosley-Thompson, and G. W. Lamorey. 2001. Accumulation Map for the Greenland Ice Sheet: 1971-1990, *Geophys. Res. Lett.*, in press.

Bamber, J.L., Ekholm, S. and Krabill, W. B. 2001. A new, high-resolution digital elevation model of Greenland fully validated with airborne laser altimeter data, *J. Geophys. Res.*, in press.

Braithwaite, R.J. 1992. Degree-day factor, energy balance, and the increased melting of the Greenland Ice Sheet under a warmer climate, *Grølands Geologiske Undersøgelse*, Rapport 155, 79-83.

Braithwaite, R.J. 1995. Positive degree-day factors for ablation on the Greenland ice sheet studied by energy-balance modelling, *J. Glaciol.* 41(137), 153-160.

Braithwaite, R.J. 1996. Models of ice-atmosphere interactions for the Greenland ice sheet, *Ann. Glaciol.*, 23, 149-153.

Braithwaite, R.J., T. Konzelmann, C. Marty, and O. Olesen. 1998. Reconnaissance study of glacier energy balance in North Greenland, 1993-1994, *J. Glaciol.* 44(147), 239-247.

Bøggild, C. E., N. Reeh and H. Oerter. 1994. Modelling ablation and mass balance sensitivity to climate change of Storstrømmen, northeast Greenland, *Global and Planetary Change* **9**, 79-90.

Chuah, T.S., S.P. Gogineni, C. Allen and B. Wohletz. 1996. Radar thickness measurements over the northern part of the Greenland Ice Sheet, *Radar Systems and Remote Sensing Laboratory Technical Report 10470-3*, University of Kansas, Lawrence, Kansas.

Davies, W.E. and D.B. Krinsey. 1962. The recent regimen of the ice cap margin in North Greenland, *in* Symposium of Bergurgl, Austria, (10-18 Sept. 1962): International Association of Scientific Hydrology, Pub. 58, 119-130.

Ekholm, S. 1996. A full coverage, high-resolution, topographic model of Greenland computed from a variety of digital elevation data. *J. Geophys. Res.* **101**(B10), 21,961–21,972.

Friedmann, A., J.C. Moore, T. Thorsteinsson, J. Kipfstuhl, and H. Fischer. 1995. A 1200 year record of accumulation from northern Greenland. *Ann. Glaciol.* 21, 19-25 pp.

Goldthwait, R.P. 1971. Restudy of Red Rock ice cliff, Nunatarssuaq, Greenland: U.S. Army Cold Regions Research and Engineering Laboratory (CRREL), Technical Report 224, 27p.

Higgins, A. K. 1988. Glacier velocities from aerial photographs in North and North-East Greenland, *Rapp. GRønlands geol. Unders.* 140, 102-105.

Higgins, A.K. and A. Weidick. 1988. The world's northernmost surging glacier, *Zeitschrift fur Gletscherkunde und Glazialgeologie* 24(2), 42-47.

Higgins, A. 1991. North Greenland glacier velocities and calf ice production. *Polar forschung*, 60(1), 1–23.

Høyt, T. 1970. Surveying and mapping in southern Peary Land, North Greenland, *Meddeleser om Grønland* 182(3), 50p.

Huybrecht, P. 1990. A 3-D model for the Antarctic ice sheet: a sensitivity study on the glacial-interglacial contrast, *Climate Dyn.* 5, 79-92.

Huybrecht, P. and J. de Wolde. 1999. The dynamic response of the Greenland and Antarctic ice sheets to multiple-century climatic warming, *J. Climate* 12(8), 2169-2188.

Jacobs, S.S., H.H. Helmer and A. Jenkins. 1996. Antarctic ice sheet melting in the southeast pacific. *Geophys. Res. Lett.* **23**(9), 957–960.

Jenkins, A. and C.S.M. Doake 1991. Ice-ocean interaction on Ronne Ice Shelf, Antarctica. *J. Geophys. Res.*, **96**(C1), 791–813.

Joughin, I., D.P. Winebrenner and M.A. Fahnestock. 1995. Observations of ice-sheet motion in Greenland using satellite radar interferometry. *Geophys. Res. Lett.*, **22**(5), 571–574.

Joughin, I., S. Tulaczyk, M. Fahnestock and R. Kwok. 1996. A mini-surge on the Ryder glacier, Greenland, observed by satellite radar interferometry. *Science* **274**(5285), 228–230.

Joughin, I., R. Kwok and M.A. Fahnestock. 1998. Interferometric estimation of three-dimensional ice-flow using ascending and descending passes, *IEEE Trans. Geosc. Rem. Sens.* 36(1), 25-37.

Joughin, I., M. Fahnestock, R. Kwok, P. Gogineni, and C. Allen. 1999. Ice flow of Humboldt, Petermann and Ryder Gletscher, northern Greenland, *J. Glaciol.*, 45(150), 231-241.

Joughin, I. M. Fahnestock, D. McAyeal, J. Bamber and P. Gogineni. Observation and analysis of ice flow in the largest Greenland ice stream, *J. Geophys. Res.*, this issue.

Koch, L. 1928. Contributions to the glaciology of North Greenland, *Meddelelser om Grønland* 65, part 2, 181-464.

Kollmeyer, R.C. 1980. West Greenland outlet glaciers: An inventory of the major iceberg producers, in *World Glacier Inventory, Proceedings of the Workshop at Riederalp, Switzerland, 17-22 September 1978*, International Association of Hydrological Sciences, Publication No. 126, p. 57–65.

Konzelmann, T. and R. Braithwaite. 1995. Variations of ablation, albedo and energy balance at the margin of the Greenland Ice Sheet, Kronprins Christian Land, eastern North Greenland, *J. Glaciol.* **41**(137), 174-182.

Krabill, W. and 8 others. 1999. Rapid thinning of the southern Greenland Ice Sheet, *Science*, 283(5407) 1522-1524.

Lister, H. 1958. Glaciology, 1: the balance sheet or mass balance, *in* Hamilton, R.A., ed., Venture to the Arctic: Pelican Books, A 432, p. 167-188.

Mock, S.J. 1966. Fluctuations of the terminus of Harald Moltke Brae, Greenland, *J. Glaciol.*, 6(45), 369-373.

Mohr, J.J., N. Reeh and S.N. Madsen. 1998. Three-dimensional glacial flow and surface elevation measured with radar interferometry, *Nature* 391, 273-276.

Nobles, L.H. 1960. Glaciological investigations, Nunatarssuaq ice ramp, north-western Greenland: U.S. Army Snow, Ice and Permafrost Research Establishment, U.S. Army Cold Regions Research and Engineering Laboratory (CRREL) Technical Report 66, 57p.

Ohmura, A. and N. Reeh. 1991. New precipitation and accumulation maps for Greenland. *J. Glaciol.* **37**(125), 140–148.

Le Provost, C., F. Lyard, J.M. Molines, M.L. Genco and F. Rabilloud. 1998. A Hydrodynamic Ocean Tide Model Improved by assimilating a satellite altimeter-derived data set. *J. Geophys. Res.* **103** (C3), 5513–5529.

Reeh, N. 1985. Greenland ice sheet mass balance and sea-level change, *in* Glaciers, ice sheets, and sea-level: Effects of a CO_2-induced climatic change, report of a workshop held in Seattle, Washington, 13-15 Sept. 1984: Washington, D.C., National Academy Press, 155–171.

Reeh, N. 1991. Parametrization of melt rate and surface temperature on the Greenland Ice Sheet. *Polarforschung* **59**(3), 1989, 113–128.

Reeh, N., C. E. Bøggild, and H. Oerter. 1994. Surge of Storstrømmen, a large outlet glacier from the inland ice of north-east Greenland, *Rapp. Grønlands geol. Unders.* 162, 201-209.

Reeh, N., C. Mayer, H. Miller, H.H. Thomsen and A. Weidick. 1999. Present and past climate control on fjord glaciations in Greenland: implications for IRD-deposition in the sea, *Geophys. Res. Lett.* 26(8), 1039-1042.

Rignot, E., K. Jezek and H.G. Sohn. 1995. Ice flow dynamics of the Greenland Ice Sheet from SAR Interferometry. *Geophys. Res. Lett.*, **22**(5), 575–578.

Rignot, E., S. Gogineni, W. Krabill and S. Ekohlm. 1997a. Ice discharge from north and northeast Greenland as observed from satellite radar interferometry, *Science*, 276, 934-937.

Rignot, E., S. Gogineni, W. Krabill and S. Ekohlm. 1997b. Mass balance of north Greenland - Response, *Science*, 278(5336), 209.

Rignot, E. 1996. Tidal flexure, ice velocities and ablation rates of Petermann Gletscher, Greenland, *J. Glaciol.*, 42(142), 476-485.

Rignot, E. 1998a. Hinge-line migration of Petermann Gletscher, north Greenland, detected using satellite radar interferometry, *J. Glaciol.*, 44, 469-476.

Rignot, E. 1998b. Radar Interferometry Detection of Hinge-Line Migration on Rutford Ice Stream and Carlson Inlet, Antarctica, *Ann. Glaciol.*, 27, 25-32.

Rignot, E., G. Buscarlet, B. Csatho, S.P. Gogineni, W.B. Krabill and M. Schmeltz. 2000. Mass balance of the northeast sector of the Greenland ice sheet: a remote sensing perspective, *J. Glaciol.*

46(153), in press.

Smith, A.M. 1991. The use of tiltmeters to study the dynamics of Antarctic ice-shelf grounding lines. *J. Glaciol.*, **37**(125), 51–58.

Thomas, R. H. and 9 others. 2000. Substantial thinning of a major east Greenland outlet glacier, *Geophys. Res. Lett.*, 27(9), 1291.

Thomsen, H.H., N. Reeh, O.B. Olesen, C.E. Bøggild, W. Starzer, A. Weidick and A.K. Higgins. 1997. *Geol. Greenland Survey Bull.* 176, 95-103.

van de Wal, R.S.W. 1996. Mass-balance modelling of the Greenland ice sheet; a comparison of an energy-balance and a degree-day model, *Ann. Glaciol.* 23, 36-45.

Weidick, A. 1995. Greenland. *U.S. Geol. Surv. Prof. Pap. 1386*, (Denver, CO, 1995), C1–C105.

Figure 1. ERS SAR mosaic of northern Greenland glaciers, on a polar stereographic grid (courtesy NSIDC, complemented by data from this project). ISR lines used to calculate fluxes are shown in red; grounding lines from 1996 are green; drainage basins are black; DEM contour lines (every 100 m from 100 m to 2000 m and every 200 m thereafter) are blue. JG = Jungersen Gletscher; HG = Henson Gletscher; MSG = Marie Sophie Gletscher; and LB = L. Bistrup Brae. ©ESA 1996.

Figure 2. Vector velocity map of Petermann Gletscher derived from ERS InSAR ascending and descending tracks. The grounding line is shown in white for 1996, and black for 1992. Flow vectors are red. Velocity contours are blue. ISR lines are green. Vector velocity maps for Ryder Gletscher, Nioghalvfjerdsbrae and Zachariae Isstrøm, and Storstrømmen are shown, respectively, in *Joughin et al.* [1998], *Rignot et al.*, [2000], and *Mohr et al.* [1998].

Figure 3. Along-flow surface and bed elevations of (a) Petermann Gletscher on May 10, 1999; (b) Ryder Gletscher on May 23, 1999; (c) Nioghalvfjerdsbrae on May 19, 1999; and (d) Zachariae Isstrøm on May 19, 1999. Surface elevations are from ATM (dotted line) and DEM (continuous line). Thicknesses are from ISR (thin line), deduced from hydrostatic equilibrium from ATM (thick, bold line) and corrected-DEM elevations (continuous line). Grounding-line positions are marked with a diamond symbol. The point of first hydrostatic equilibrium of the ice is at the crossing of the ISR thickness with the ATM-derived thickness, coming from upstream.

Figure 4. Grounding-line migration measured with InSAR between 1992 and 1996 on (a) Humboldt Gletscher (b) Petermann Gletscher; (c) Steensby Gletscher; (d) Ryder Gletscher; (e) C. H. Ostenfeld Gletscher; (f) Hagen Brae; (g) Nioghalvfjerdsbrae; (h) Zachariae Isstrøm (no 1992 InSAR); (i) Storstrømmen and L. Bistrup Brae. The location of the grounding line is shown in black for 1992 and white for 1996, and marked with a pointing arrow. ISR lines are shown in white for 1995, and black for 1999. Intercepts between grounding lines and ISR are marked as diamonds. Thick, continuous lines in (b, c, d, f, g, h, i) denote portions of the ISR track for which ice is in

hydrostatic equilibrium, in white for 1995 and black for 1999. (b) includes a 1999 transverse ISR line used to estimate the grounding-line ice flux; no ATM elevation was available for that flight due to cloud cover. All plots are overlay on the radar brightness of the scene. ©ESA 1996.

Table 1. Glacier thickness (m) at the grounding line. S = south, C = center, N = north sector of the grounding line. H_{ISR} = ISR thickness; H_{DEM} = h_{DEM} x 9.115; h_{DEM} = DEM surface elevation; h_{ATM} = ATM surface elevation; $\bar{H}_{DEM}$ = corrected thickness from DEM. * ice shelf with elevation anomaly.

Glacier/Year	H_{ISR}	H_{DEM}	$h_{DEM-AOL}$	H_{ISR}/H_{AOL}	$\bar{H}_{DEM}$
Petermann Gl. 95	544±2	654±18	+5±1	9.7±1.1	554
Petermann Gl. 99	550±3	649±16	+5±2	9.5±1.3	549
Ryder Gl. 97	406±6	480±6	+16±1	10.8±0.5	400
Hagen Brae* 99	173±25	638±48	+48±2	8.8±1.0	193
Nioghalvfjerdsbrae 95S	639±2	619±3	+0±0	10.3±1.0	683
Nioghalvfjerdsbrae 99C	744±1	614±13	-12±0	10.3±0.7	678
Zachariae Isstrøm 99N	564±2	648±28	+21±1	10.9±1.3	584
Zachariae Isstrøm 99S	527±35	598±38	+14±1	10.9±1.3	525
Storstrømmen 97	422±3	441±2	+10±1	11.1±0.4	441
Storstrømmen 99	507±2	1143±3	+13±0	11.0±0.4	N.A.
L. Bistrup Brae 97	391±19	361±22	-19±10	11.1±0.4	N.A.
L. Bistrup Brae 99	452±10	773±16	+16±1	11.0±0.4	N.A.

Table 2. Equilibrium line altitude (ELA): P = published estimate; ERS = estimate from ERS data; M = estimate from degree day model; DDF = Degree-day factor for ice/now (mm/^{o}C/d) used in the model. Sources: [1] *Nobles* [1960]; [2] *Weidick* [1995]; [3] *Koch* [1928]; [4] *Bøggild et al.* [1994].

Glacier	ELA P	ELA ERS	ELA M	DDF
Harald Molke Br.	900[1]	700	720	9.8/3.0
Heilprin/Leidy/Marie Gl.	900[1]	900	803	9.8/3.0
Tracy Gl.	900[1]	900	948	9.8/3.0
Humboldt Gl.	600-800[1]	700	733	6.9/2.1
Petermann Gl.	800-900[2,3]	800	747	9.8/3.0
Ryder /Steensby Gl.	800[2]	800	768	9.8/3.0
C.H. Ostenfeld Gl.	N.A.	800	710	9.8/3.0
Academy Gl.	900-1000[2]	800	954	9.8/3.0
Hagen Brae	N.A.	800	954	9.8/3.0
Nioghalvfjerdsbrae	N.A.	800	937	4.9/1.5
Zachariae Isstrøm	N.A.	800	1002	4.9/1.5
Storstrømmen	1100[4]	1100	1170	9.8/3.0
L. Bistrup Br.	N.A.	1000	1086	9.8/3.0

Table 3. Mass balance at the ISR flux gate. V = center velocity (m a^{-1}); T = center thickness (m); IF = ISR flux (km^3 ice a^{-1}); AA = drainage area above ISR flux gate (km^2); AC, AB, BF, MB = accumulation, ablation, balance flux, and mass balance, respectively (km^3 ice a^{-1}). The last row shows the total for each column.

Glacier	V	T	IF	AA	AC	AB	BF	MB
Heilprin Gl.	548	1036	2.19	7083	1.71	0.05	1.66	-0.53
Tracy Gl.	516	1213	1.43	2969	0.68	0.13	0.55	-0.88
Humboldt Gl.	350	500	6.25	44214	8.56	2.42	6.14	-0.11
Petermann Gl.	553	1050	12.82	68573	12.41	0.19	12.21	-0.61
Ryder Gl.	270	1100	3.88	27836	4.75	0.06	4.69	+0.81
Ostenfeld Gl.	153	800	2.32	8573	1.50	0.00	1.50	-0.82
Academy Gl.	150	1200	0.69	9561	1.39	0.01	1.38	+0.69
Hagen Br.	130	1100	1.03	10057	1.52	0.01	1.50	+0.47
Nioghalvfjerdsbrae	1250	700	14.27	96093	12.54	1.12	11.41	-2.86
Zachariae Is.	500	800	11.65	92095	13.12	1.51	11.61	-0.04
Storstrømmen	230	1040	5.80	51465	7.80	0.03	7.77	+1.97
			62.3	418519	66.0	5.5	60.4	-1.9

Table 4. Mass balance at the grounding line (GL). V = center velocity (km a^{-1}); T = center thickness (m); GF = grounding line flux (km^3 ice a^{-1}); CF = calving flux (km^3 ice a^{-1}); AA = accumulation area above grounding line (km^2); AC, AB, BF, MB = accumulation, ablation, balance flux and mass balance, respectively (km^3 ice a^{-1}). Sources: * *Higgins*, [1991]; + *Reeh et al.* [1994]

Glacier	V	T	GF	CF	AA	AC	AB	BF	MB
Petermann Gl.	1160	630	11.67	0.59*	69706	12.71	1.82	10.89	-0.78
Steensby Gl.	270	460	0.51	0.26	3040	0.73	0.16	0.57	+0.06
Ryder Gl.	540	620	2.29	0.66*	28707	4.95	0.91	4.04	+1.75
C.H. Ostenfeld Gl.	810	600	2.27	0.54*	9481	1.67	0.34	1.33	-0.94
Hagen Br.	61	200	0.07	0.36*	10629	1.61	0.57	1.04	+0.97
Nioghalvfjerdsbrae	1300	650	14.19	0.90	96309	12.56	1.42	11.14	-3.05
Zachariae Is.	1100	550	10.81	1.10	92680	13.19	2.34	10.85	+0.04
Storstrømmen	15	530	0.03	0.90+	54605	8.37	7.09	1.28	+1.25
			41.8	5.37	365157	55.7	14.7	41.1	-0.7

Table 5. Steady-state basal melting rates of the floating glacier tongues in northern Greenland (m ice a^{-1}). Positive values indicate melt. NB = Ice-shelf net mass balance (m ice a^{-1}) between GL and ice front, equal to CF minus GF in Table 4 divided by the ice-shelf area indicated in parenthesis (km^2); AB = Ablation plus accumulation (km^3 ice a^{-1}); BM = Average basal melt rate (m ice a^{-1}); NB_{10} = Ice-shelf net mass balance between GL and flux gate located 10 km downstream, with ice-shelf area indicated in parenthesis; AB_{10} = Ablation plus accumulation; BM_{10} = basal melt rate for first 10-km of floating ice.

Glacier	NB	AB	BM	NB_{10}	AB_{10}	BM_{10}
Petermann Gletscher	-8.4 (1304)	-2.2	6	-24.0 (263)	-2.2	22
Steensby Gletscher	-7.1 (36)	-1.2	6	N.A.	N.A.	N.A.
Ryder Gletscher	-10.0 (245)	-1.6	8	-26.4 (101)	-1.5	25
C.H. Ostenfeld Gl.	-12.6 (137)	-1.1	11	-26.9 (49)	-1.1	26
Nioghalvfjerdsbrae	-6.5 (1874)	-1.3	5	-27.7 (318)	-1.3	26
Zachariae Isstrøm	-10.0 (1065)	-1.5	8	-27.1 (170)	-1.5	25

Table 6. Grounding line migration. 1992 = latitude/longitude (deg) of 1992 GL crossing with ISR; 1996 = latitude/longitude of 1996 GL crossing with ISR; δx = horizontal migration between 1992 and 1996 (m), negative means retreat; α = surface slope (percent), positive upwards; β = bed slope (percent), positive upwards; δh = ice thinning rate (m a^{-1}) between 1992 and 1996 deduced from retreat rate; δs = ice thinning rate (m a^{-1}) obtained with ATM between 1994 and 1999. Sources: [1] *Rignot* [1998a]; [2] *Rignot et al.* [2000].

Glacier	1992	1996	δx	α	β	δh	δs
Humboldt Gletscher	79.683/-64.43	79.682/-64.39	-780	-1.1	+1.0	-1.7	-1.0±0.5
Petermann Gletscher[1]	80.562/-59.89	80.559/-59.88	-450	-1.0	-1.0	-1.3	N.A.
Steensby Gletscher	81.470/-54.41	81.469/-54.44	+105	-0.8	-0.7	+0.2	N.A.
Ryder Gletscher	81.619/-50.48	81.581/-50.44	-4200	-0.5	+1.0	-4.0	-1.0±0.6
Ostenfeld Gletscher	81.600/-45.29	81.595/-45.27	-500	-1.0	N.A.	-1.2	N.A.
HagenBrae	81.439/-27.45	81.437/-27.47	-390	-2.2	+5.6	-1.6	-2.5±1.5
Nioghalvfjerdsbrae E[2]	79.274/-22.37	79.270/-22.38	-450	-0.9	-3.2	-1.5	N.A.
Nioghalvfjerdsbrae C[2]	79.361/-22.46	79.357/-22.49	-650	-1.2	+0.7	-1.7	N.A.
Zachariae Isstrøm	N.A.	78.910/-20.61	N.A.	N.A.	N.A.	N.A.	-0.3±0.3
Storstrømmen 99S	76.730/-22.72	76.724/-22.72	+658	-0.4	+0.4	+0.6	-2±0.5
Storstrømmen 97N	76.760/-22.61	76.773/-22.60	-1395	-0.1	+0.6	0.0	N.A.
L. Bistrup Brae 99W	76.679/-22.74	76.651/-22.82	+3708	+0.5	-0.5	+4.0	+0.5±1
L. Bistrup Brae 97E	76.666/-22.68	76.639/-22.69	+3092	-1.0	+0.7	+7.0	N.A.

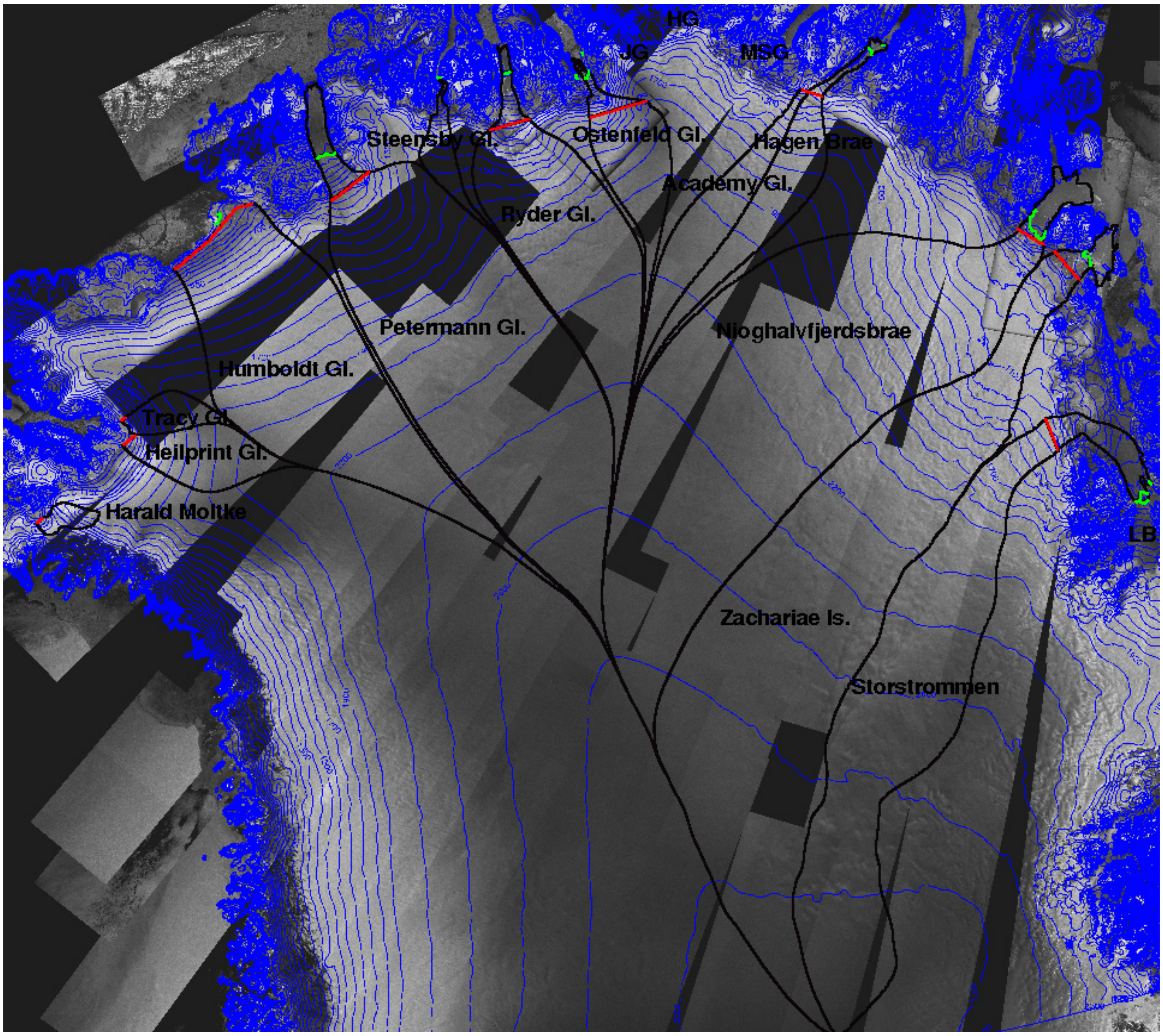
HG
JG
MSG
Steensby Gl.
Ostenfeld Gl.
Hagen Brae
Academy Gl.
Ryder Gl.
Petermann Gl.
Nioghalvfjerdsbrae
Humboldt Gl.
Tracy Gl.
Heilprint Gl.
Harald Moltke
LB
Zachariae Is.
Storstrommen

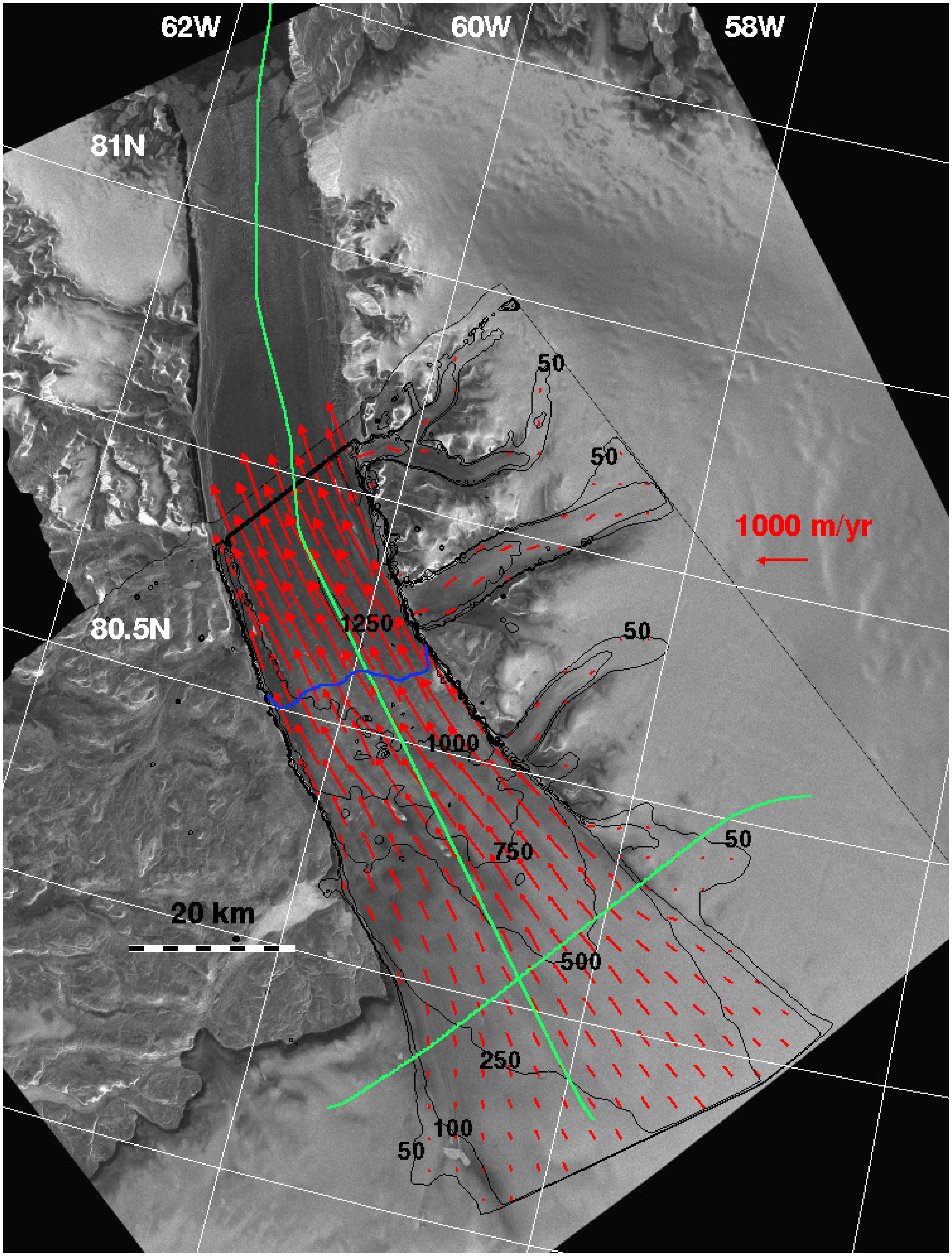
62W
60W
58W
81N
80.5N
50
50
1000 m/yr
1250
50
1000
750
50
20 km
500
250
100
50

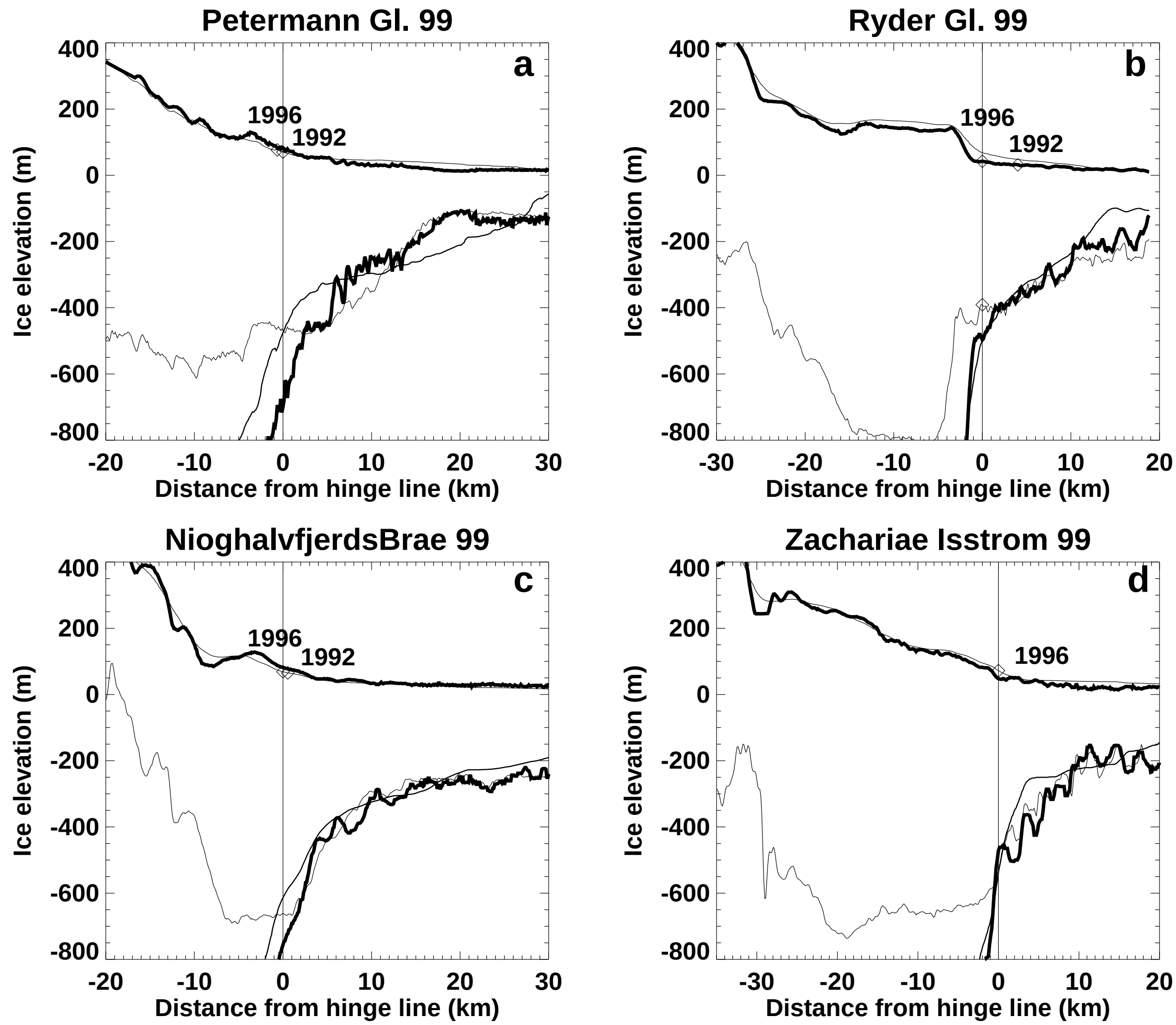
Petermann Gl. 99
a
1996
1992
Ice elevation (m)
Distance from hinge line (km)
Ryder Gl. 99
b
1996
1992
NioghalvfjerdsBrae 99
c
1996
1992
Zachariae Isstrom 99
d
1996

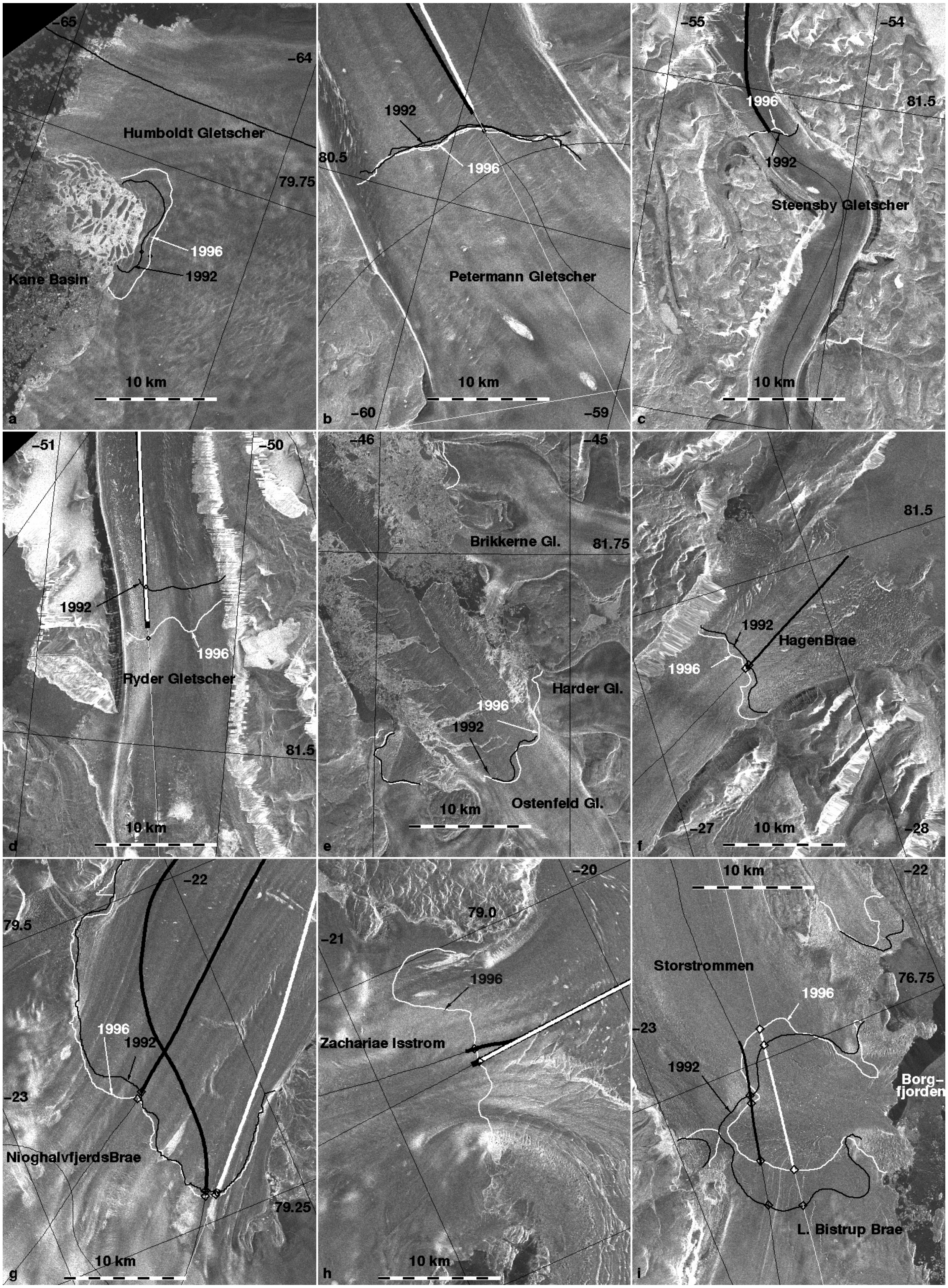
-65
-64
Humboldt Gletscher
79.75
1996
1992
Kane Basin
10 km
a
1992
80.5
1996
Petermann Gletscher
10 km
b
-60
-59
-55
-54
1996
81.5
1992
Steensby Gletscher
10 km
c
-51
-50
1992
1996
Ryder Gletscher
81.5
10 km
d
-46
-45
Brikkerne Gl.
81.75
Harder Gl.
1996
1992
Ostenfeld Gl.
10 km
e
81.5
1992
HagenBrae
1996
-27
10 km
-28
f
-22
79.5
1996
1992
-23
NioghalvfjerdsBrae
79.25
10 km
g
-20
79.0
-21
1996
Zachariae Isstrom
10 km
h
10 km
-22
Storstrommen
76.75
1996
-23
1992
Borg-
fjorden
L. Bistrup Brae
i